

# Direct torque control of induction motor based on double-power-super-twisting sliding mode speed control for electric vehicle applications

Siham Mencou, Majid Ben Yakhelf, Elbachir Tazi

Engineering Sciences Laboratory, Polydisciplinary Faculty of Taza, Sidi Mohamed Ben Abdellah University, Fez, Morocco

## Article Info

### Article history:

Received Nov 11, 2023

Revised Jan 26, 2024

Accepted Feb 2, 2024

### Keywords:

Electric vehicle

Direct torque control

Double-power-super-twisting

sliding mode control

Induction motor

## ABSTRACT

To improve the performance and energy efficiency of the direct torque control of induction motors used in electric vehicles a double-power-super-twisting sliding mode control (DPSTA.SMC) strategy has been introduced in the closed speed loop. This strategy is based on the novel double-power-super-twisting algorithm (DPSTA), which combines the performance of the traditional super-twisting algorithm (STA) with the double power reaching law (DPRL). The stability of the algorithm has been proven using a quasi-quadratic Lyapunov function. The performances of the proposed DPSTA.SMC controller have been compared with that of PI, fuzzy logic, and STA.SMC controllers. Detailed simulations are carried out using MATLAB/Simulink software. The results demonstrate that this approach effectively improves tracking accuracy, system robustness and energy efficiency, while significantly reducing the chattering phenomenon.

*This is an open access article under the [CC BY-SA](https://creativecommons.org/licenses/by-sa/4.0/) license.*



## Corresponding Author:

Siham Mencou

Engineering Sciences Laboratory, Polydisciplinary Faculty of Taza, Sidi Mohamed Ben Abdellah University  
Fes, Morocco

Email: [siham.mencou@usmba.ac.ma](mailto:siham.mencou@usmba.ac.ma)

## 1. INTRODUCTION

Because of global warming, the energy crisis, and other environmental issues, as well as skyrocketing fuel prices, the automotive industries are promoting electric vehicles (EVs). In addition to zero emissions, EVs have superior efficiency and quicker controlled torque in contrast to internal combustion engine (ICE) vehicles [1], [2]. Various types of electric motors have been suggested for EV propulsion [3], [4]. Among these, the induction motor (IM) is the best solution to meet the main requirements of EV drive due to its reliability, affordability, robustness, and minimal maintenance costs [5]-[7]. However, the analytical model of the IM is non-linear, strongly related and multi-variable [7], [8]. This complicates its control and requires more advanced control algorithms to achieve the required performance in electric drive, including fast torque response, wide speed control range, high reliability and robustness for various vehicle operating conditions, and high efficiency [2]-[8]. The IM can exhibit exceptional dynamic response performance when operated with the direct torque control (DTC) strategy [9], [10]. It presents more advantages such as a fast response and less dependence on the machine parameters [11]-[12]. In the conventional DTC system, the PI controller is commonly employed for the speed loop due to its ease of implementation and its simplicity. However, since the VE with IM is a strongly linked and multivariate nonlinear system it is difficult to achieve an ideal control effect using the PI control strategy [7]. Therefore, various nonlinear control techniques have been proposed to replace PI controllers, such as fuzzy control, model predictive control and artificial neural networks [13]-[16].

Sliding mode control (SMC) has gained increasing interest due to its relatively simple design, guaranteed stability, and high robustness against parameter and external disturbances [17]-[19]. However, its chattering problem cannot be ignored, which can lead to significant overheating of the motor windings [20]-[22]. In the literature, different types of algorithms have been made to overcome this problem. Among them are boundary layer solutions, the reaching law approach, and high-order algorithms [23], [24]. The super-twisting algorithm (STA) is one of the high-order sliding mode algorithms (SMA) that has been used to ensure high robustness while significantly weakening the chattering effect [24]-[26]. Although STA can eliminate the chattering phenomenon, since the proportional term in the scheme is the square root calculation of the sliding variable, it significantly reduces the convergence speed and the ability to reject disturbances of the algorithm [27], [28].

To overcome these challenges, we propose in this work a new double-power-super-twisting algorithm (DPSTA), which combines the advantages of the STA algorithm and the double-power reaching law (DPRL). Our main contribution is to apply DTC control using the speed controller based on the DPSTA\_SMC algorithm, in order to improve the robustness, performance and efficiency of the IM used to drive EVs. The performance of the proposed controller is demonstrated through critical and comparative simulations with the PI, STA\_SMC and FLSC controllers using MATLAB/Simulink software. This article is organized on five sections: In section 2 we present the double-power-super-twisting algorithm (DPSTA). Next, in section 3 we establish the system modeling and simulation method. Simulation results and their interpretation are given in section 4. Finally, the conclusion is presented at the end of the paper.

## 2. DOUBLE POWER SUPER TWISTING ALGORITHM (DPSTA)

### 2.1. Super-twisting algorithm (STA)

The STA (introduced by Levant [29], [30]) is one of the most extensively applied second-order SMAs. This algorithm is specifically applicable to systems of the first relative degree to reduce the chattering phenomenon [31]. The basic form of this algorithm is written as (1):

$$\begin{cases} \frac{dx_1}{dt} = -k_1 |x_1|^{\frac{1}{2}} \text{sign}(x_1) + x_2 + \varphi_1(x_1, t) \\ \frac{dx_2}{dt} = -k_2 \text{sign}(x_1) + \varphi_2(x_2, t) \end{cases} \quad (1)$$

where  $(x_1, x_2)$ ,  $(k_1, k_2)$ , and  $(\varphi_1(x_1, t), \varphi_2(x_2, t))$  are the scalar state variables, the sliding-mode gains, and the perturbation terms.

If there exist constant  $\delta_1 \geq 0$  such that:

$$|\varphi_1(x_1, t)| \leq \delta_1 |x_1|^{\frac{1}{2}} \quad \text{and} \quad \varphi_2(x_2, t) = 0 \quad ; \quad \forall t \geq 0 \quad (2)$$

the equilibrium point  $x(0, 0)$  exhibits strong global asymptotic stability provided that the sliding-mode gains meet the specified condition [31].

$$\begin{cases} k_1 > 2\delta_1 \\ k_2 > k_1 \frac{5\delta_1 k_1 + 4\delta_1^2}{2(k_1 - 2\delta_1)} \end{cases} \quad (3)$$

### 2.2. The double power sliding mode reaching law (DPSMRL)

The DPSMRL is designed to enhance the reaching speed and dynamic quality of the SMC system, even when the system is far away from the sliding mode surface [32], [33]. The DPSMRL can be expressed as (4):

$$\dot{s} = -\lambda_1 |s|^{\gamma_1} \text{sign}(s) - \lambda_2 |s|^{\gamma_2} \text{sign}(s) \quad (4)$$

where  $\lambda_1 > 0$ ;  $\lambda_2 > 0$ ;  $0 < \gamma_1 < 1$  and  $\gamma_2 > 1$ .

### 2.3. Double power super twisting algorithm (DPSTA)

To enhance the convergence speed and robustness of the sliding mode control system, we propose a novel DPSTA in this paper. The DPSTA combines the advantages of two algorithms STA and DPSMRL. Our

approach involves replacing the switching function in the STA with DPSMRL:

$$\begin{cases} \frac{dx_1}{dt} = -k_1\phi_1(x_1) + x_2 + \varphi_1(x_1, t) \\ \frac{dx_2}{dt} = -k_2\phi_2(x_1) + \varphi_2(x_2, t) \end{cases} \quad (5)$$

with:

$$\begin{cases} \phi_1(x) = |x|^{1/2} \text{sign}(x) + \lambda|x|^{3/2} \text{sign}(x) \\ \phi_2(x) = \phi_1^2(x)' = 2\phi_1(x) \cdot \phi_1(x)' = \text{sign}(x) + 4\lambda|x| \text{sign}(x) + \frac{3}{2}\lambda^2|x|^2 \text{sign}(x) \end{cases} ; \lambda \geq 0 \quad (6)$$

### 2.3.1. Stability analysis

The stability of the system (5) is established by the following theorem:

– Theorem:

If for constants  $\delta_1 \geq 0$  and  $\xi_1 = \frac{1}{\phi_1'(x_1)}$ :

$$|\varphi_1| \leq \delta_1 |\zeta_1| \quad \text{and} \quad \varphi_2 = 0 ; \forall t \geq 0 \quad (7)$$

Then the sliding-mode gains  $k_1$  and  $k_2$  satisfy the conditions:

$$\begin{cases} k_1 > 2\delta_1 \\ k_2 > k_1 \frac{5\delta_1 k_1 + 4\delta_1^2}{2(k_1 - 2\delta_1)} \end{cases} \quad (8)$$

System converge to the equilibrium point  $x(0, 0)$  in finite time.

– Proof:

The stability of the system can be verified using the quasi-quadratic Lyapunov function given as (9):

$$V(x, t) = \xi^T P \xi \quad (9)$$

with  $P$  the positive definite symmetric matrix  $P = \begin{bmatrix} 2k_2 + \frac{k_1}{2} & -\frac{k_1}{2} \\ -\frac{k_1}{2} & 1 \end{bmatrix}$  and  $\xi = \begin{bmatrix} \phi_1(x_1) \\ x_2 \end{bmatrix}$ . The derivative of  $\xi$  is:

$$\dot{\xi} = \frac{1}{\zeta_1} A \xi + \frac{\varphi_1}{\zeta_1} E_1 + \varphi_2 E_2 \quad (10)$$

with  $A = \begin{bmatrix} -k_1 & 1 \\ -2k_2 & 0 \end{bmatrix}$ ,  $E_1 = \begin{bmatrix} 1 \\ 0 \end{bmatrix}$ , and  $E_2 = \begin{bmatrix} 0 \\ 1 \end{bmatrix}$ . The derivative of  $V$  along the trajectory of system (5):

$$\begin{aligned} \dot{V}(x, t) &= \dot{\xi}^T P \xi + \xi^T P \dot{\xi} = \frac{1}{\zeta_1} \xi^T (A^T P + P A) \xi + \frac{\varphi_1}{\zeta_1} (E_1^T P \xi + \xi^T P E_1) + \varphi_2 (E_2^T P \xi + \xi^T P E_2) \\ &= \frac{1}{\zeta_1} \xi^T (A^T P + P A) \xi + \frac{\varphi_1}{\zeta_1} q_1^T \xi + \varphi_2 q_2^T \xi \end{aligned}$$

with  $q_1 = \begin{bmatrix} 4k_2 + k_1^2 \\ -k_1 \end{bmatrix}$  and  $q_2 = \begin{bmatrix} -k_1 \\ 2 \end{bmatrix}$ .

Then:

$$\frac{\varphi_1}{\zeta_1} q_1^T \xi \leq \frac{\delta_1}{|\zeta_1|} \xi^T \Delta \xi \quad (11)$$

where:  $\Delta = \begin{bmatrix} 4k_2 + k_1^2 & 2k_1 \\ 2k_1 & 0 \end{bmatrix}$ . So, if:  $|\varphi_1| \leq \delta_1 |\zeta_1|$  and  $\varphi_2 = 0$  :

$$\dot{V}(x, t) \leq -\frac{1}{|\zeta_1|} \xi^T Q \xi \quad (12)$$

with:

$$Q = -(A^T P + P A + \Delta) = \begin{bmatrix} k_1 (2k_2 + k_1^2) - (4k_2 + k_1^2) \delta_1 & -k_1^2 - 2\delta_1 k_1 \\ -k_1^2 - 2\delta_1 k_1 & k_1 \end{bmatrix} \quad (13)$$

$\dot{V}$  is negative definite if  $Q > 0$ , this is the case if:

$$\begin{cases} k_1 (2k_2 + k_1^2) - (4k_2 + k_1^2) \delta_1 > 0 \\ k_1 (k_1 (2k_2 + k_1^2) - (4k_2 + k_1^2) \delta_1) > (k_1^2 + 2\delta_1 k_1)^2 \end{cases} \quad (14)$$

It is easy to see that this is the case if the gains  $k_1$  and  $k_2$  satisfy the condition in (8). Then the state converges to  $x(0, 0)$  in finite time  $T = \frac{2V^{\frac{1}{2}}(x)}{\gamma(P, Q)}$  where  $\gamma(P, Q) = \frac{\lambda_{\min}^{\frac{1}{2}}\{P\} \cdot \lambda_{\min}\{Q\}}{\lambda_{\max}\{P\}}$ .

#### 2.4. Design of DPSTA\_SMC speed controller of IM

The mechanical equation of IM, with associated parameter uncertainty terms, can be expressed as (15):

$$\dot{\omega}_m = (a + \Delta a) T_{em} - (b + \Delta b) \omega_m - (f + \Delta f) \quad (15)$$

where  $\Delta a$ ,  $\Delta b$  and  $\Delta f$  represents the uncertainties of the terms  $a$ ,  $b$  and  $f$  respectively. Specifically:  $a = \frac{1}{J}$ ,  $b = \frac{f_v}{J}$  and  $f(t) = \frac{T_L(t)}{J}$ .

The speed error  $e(t)$  is defined as (16):

$$e(t) = \omega_m(t) - \omega_m^*(t) \quad (16)$$

where  $\omega_m^*$  represents the reference mechanical speed of the motor. Using (15) the derivative of the error is given by (17):

$$\dot{e}(t) = \dot{\omega}_m(t) - \dot{\omega}_m^*(t) = u(t) - be(t) + d(t) \quad (17)$$

where:

$$u(t) = aT_{em}(t) - f(t) - b\omega_m^*(t) - \dot{\omega}_m^*(t) \text{ and } d(t) = -\Delta b \cdot \omega_m(t) - \Delta f(t) + \Delta a \cdot T_{em}(t).$$

The sliding surface function  $s(t)$  is defined as (18):

$$s(t) = e(t) \quad (18)$$

the derivative of the sliding surface function is (19):

$$\dot{s}(t) = \dot{e}(t) = u(t) - be(t) + d(t) \quad (19)$$

according to DPSTA, the speed controller can be designed as (20):

$$u(t) = -k_1 \left( (|x|^{\frac{1}{2}} + \lambda|x|^{\frac{3}{2}}) \text{sign}(x) \right) - \int k_2 \left( \left( 1 + 4\lambda|x| + \frac{3}{2}\lambda^2|x|^2 \right) \text{sign}(x) \right) \quad (20)$$

where  $\lambda > 0$  and  $(k_1, k_2)$  satisfy the stability condition (8).

Therefore:

$$T_{em}^* = f_v \omega_m^* + J \dot{\omega}_m^* + T_L - J \left[ k_1 \left( (|x|^{\frac{1}{2}} + \lambda|x|^{\frac{3}{2}}) \text{sign}(x) \right) + \int k_2 \left( \left( 1 + 4\lambda|x| + \frac{3}{2}\lambda^2|x|^2 \right) \text{sign}(x) \right) \right] \quad (21)$$

### 3. METHOD FOR MODELING AND SIMULATION OF THE SYSTEM

Figure 1 shows the general modeling structure of EV driven by an MI motor under the DTC control strategy. The drive cycle shows the reference speed that the vehicle must follow. The EV battery supplies energy to the motor and auxiliary devices through an electronic power inverter. The IM generates the torque necessary to power the vehicle. Vehicle dynamics describes the vehicle's resistance forces.

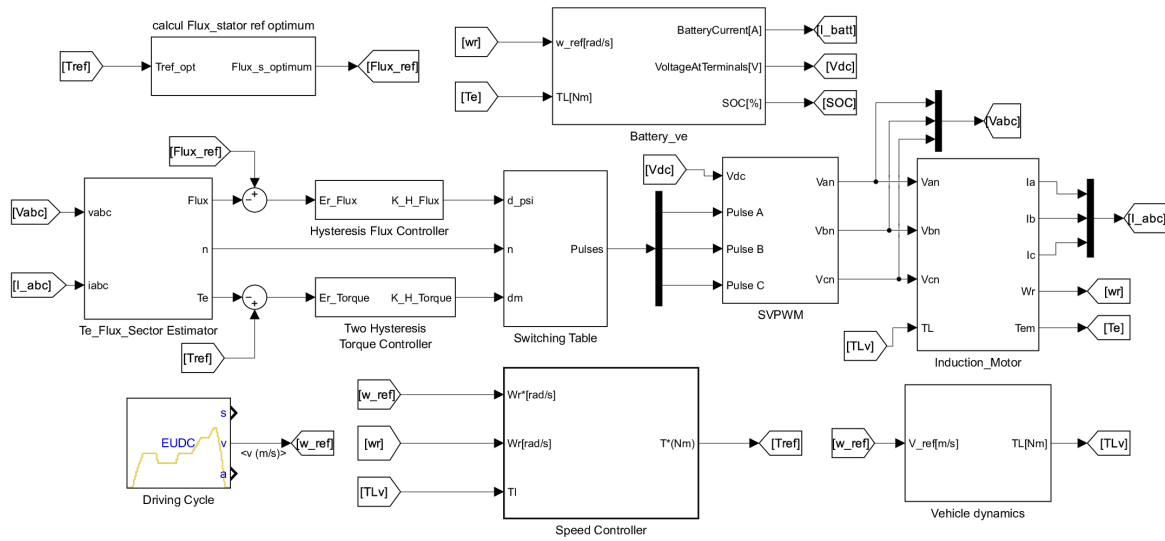


Figure 1. General system modeling structure

### 3.1. Vehicle dynamics modeling

While driving, vehicles are subject to resistance force represented by four main components: the aerodynamic resistance force ( $F_{aero}$ ), hill climbing force ( $F_{hc}$ ), rolling resistance force ( $F_{rr}$ ), and acceleration force ( $F_a$ ) [34]. When analyzing a vehicle with mass  $m$  ascending an inclined plane at a speed  $v$  and slope angle  $\alpha$ , these forces are illustrated in Figure 2.

The total resistance force is given by [34]:

$$F_{tr} = F_{rr} + F_a + F_{aero} + F_{hc} = C_{rr}mg \cos(\alpha) + 1.15ma + \frac{1}{2}\rho C_d A_f (v + v_0)^2 + mg \sin(\alpha) \quad (22)$$

where  $C_{rr}$  the rolling resistance coefficient,  $g$  is the gravity constant,  $r$  is the air density,  $A_f$  the frontal area,  $v_0$  the wind speed,  $C_d$  the aerodynamic drag constant and  $a$  is the acceleration.

As a result, the resisting torque applied to the machine in the case of a gearbox without loss and of ratio  $n$  is given by (23):

$$T_r = F_{tr} \frac{R}{n} = (C_{rr}mg \cos(\alpha) + 1.15ma + \frac{1}{2}\rho C_d A_f (v + v_0)^2 + mg \sin(\alpha)) \frac{R}{n} \quad (23)$$

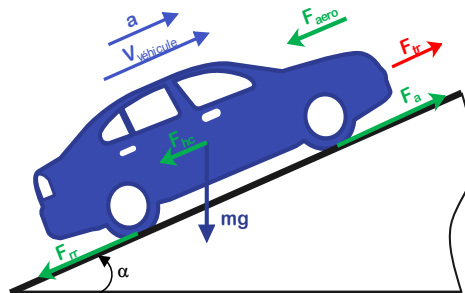


Figure 2. Force applied to the vehicle

### 3.2. Battery modeling

The battery model takes the total power demand ( $P_{total}$ ) as an input, which is then used to calculate the power demand per single cell ( $P_{Cell}$ ). This value is obtained by dividing  $P_{total}$  by the number of battery

cells ( $N_{Cell}$ ) [35]. The current demand per single cell ( $I_{Cell}$ ) is determined from  $P_{Cell}$  using the (24).

$$I_{cell} = \frac{E_{batt} - \sqrt{E_{batt}^2 - 4R_i P_{cell}}}{2R_i} \quad (24)$$

The outputs of the model are the battery terminal voltage and current, which are determined by the (25):

$$\begin{cases} I_{batt} = I_{cell} N_{cell_{parallel}} \\ V_{batt} = V_{cell} N_{cell_{serie}} \end{cases} \quad (25)$$

where  $N_{Cell_{parallel}}$  and  $N_{cell_{serie}}$  are respectively the numbers of cells in series and in parallel.

To calculate the state of charge of the battery ( $SoC$ ), the charge integration method, also known as Coulomb counting [36], is used. This method is based on the principle of conservation of charge and is particularly useful and accurate in a simulation setting. The mathematical equation for Coulomb counting is:

$$SoC = SoC_0 - \int \frac{I_{cell}(t)}{C_{cell}} dt \quad (26)$$

where  $SoC_0$  is the initial state of charge of the battery and  $C_{cell}$  is the single-cell capacity.

### 3.3. Induction motor modelling

The mathematical model of the IM in the synchronous reference frame ( $d, q$ ) is defined by (27) [37]:

$$\frac{dX}{dt} = AX + BU \quad (27)$$

$$\text{with: } X = \begin{bmatrix} i_{sd} \\ i_{sq} \\ \psi_{sd} \\ \psi_{sq} \end{bmatrix}; B = \begin{bmatrix} \frac{1}{\sigma L_s} & 0 \\ 0 & \frac{1}{\sigma L_s} \\ 1 & 0 \\ 0 & 1 \end{bmatrix}; U = \begin{bmatrix} v_{sd} \\ v_{sq} \end{bmatrix} \text{ and } A = \begin{bmatrix} -\frac{R_s + R_r}{L_s + L_r} & -\omega & \frac{R_r}{\sigma L_s L_r} & \frac{\omega}{\sigma L_s} \\ \omega & -\frac{R_s + R_r}{L_s + L_r} & -\frac{\omega}{\sigma L_s} & \frac{R_r}{\sigma L_s L_r} \\ -R_s & 0 & 0 & 0 \\ 0 & -R_s & 0 & 0 \end{bmatrix}$$

where  $\sigma = 1 - \frac{M^2}{L_s L_r}$ ,  $R_s$  and  $R_r$  the stator and rotor resistance,  $L_s$  and  $L_r$  the stator and rotor inductance,  $M$  the mutual inductance between stator phases,  $\omega$  the electric speed,  $[v_{sq} \ v_{sd}]^T$  the stator voltage components in reference ( $d, q$ ) frame,  $[\psi_{sd} \ \psi_{sq}]^T$  the stator voltage components in ( $d, q$ ) frame and  $[i_{sd} \ i_{sq}]^T$  the stator current components in ( $d, q$ ) frame.

### 3.4. The DTC control system

The block diagram of the IM driving a VE based on the DTC strategy is shown in Figure 3. This control technique uses real-time measurement of stator current and voltage to calculate the electromagnetic torque and stator flux of the machine using the following equations :

$$T_{em} = \frac{3}{2} N (\psi_{s\alpha} i_{s\beta} - \psi_{s\beta} i_{s\alpha}) \quad (28)$$

$$\psi_s = |\psi_s| e^{-j\theta_s t} \quad (29)$$

with  $|\psi_s| = \sqrt{\psi_{s\alpha}^2 + \psi_{s\beta}^2}$  and  $\theta_s = \tan\left(\frac{\psi_{s\beta}}{\psi_{s\alpha}}\right)$ . Where  $\psi_{s\alpha}$  and  $\psi_{s\beta}$  are the stator flux components of the machine in the ( $\alpha, \beta$ ) stator-related frame given by:

$$\begin{cases} \psi_{s\alpha}(t) = \int_0^t (V_{s\alpha} - R_s I_{s\alpha}) dt \\ \psi_{s\beta}(t) = \int_0^t (V_{s\beta} - R_s I_{s\beta}) dt \end{cases} \quad (30)$$

The comparison of these values with their respective reference values ( $T_{em}^*$  and  $\psi_s^*$ ) are the inputs to two hysteresis comparators. The comparison results ( $K_\psi$ ,  $K_{T_{em}}$ ) and the sector number ( $N$ ) present the switching table inputs (Table 1). The table allows for the selection of the voltage vector that will be applied to the machine, and the inverter control signal sequences ( $S_a$ ,  $S_b$ , and  $S_c$ ).

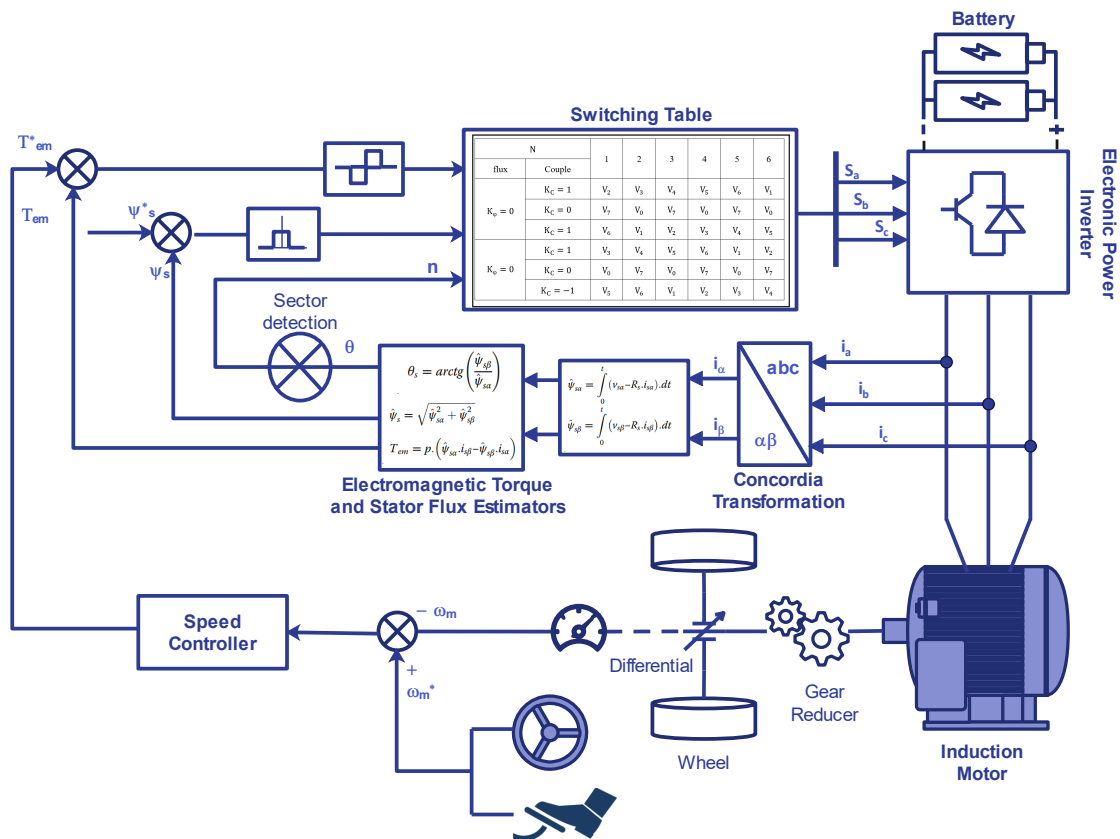


Figure 3. DTC control of the vehicle’s induction motor

Table 1. DTC switching table

$K_{\psi}$	$N$ $K_{tem}$	1	2	3	4	5	6
		1	$V_2$	$V_3$	$V_4$	$V_5$	$V_6$
1	0	$V_7$	$V_0$	$V_7$	$V_0$	$V_7$	$V_0$
	-1	$V_6$	$V_1$	$V_2$	$V_3$	$V_4$	$V_5$
0	1	$V_3$	$V_4$	$V_5$	$V_6$	$V_1$	$V_2$
	0	$V_0$	$V_7$	$V_0$	$V_7$	$V_0$	$V_7$
	-1	$V_5$	$V_6$	$V_1$	$V_2$	$V_3$	$V_4$

#### 4. RESULT AND ANALYSIS

The performances analysis of the DPSTA.SMC speed controller are evaluated using simulations in the MATLAB/Simulink software. All simulations are performed with a sampling interval of 2 ms, corresponding to a switching frequency of 500 Hz. The model parameters used in the simulation are shown in Table 2. To test the performance of the proposed controller, we compared it to the fuzzy logic speed controller (FLSC) used in [16] and to PI and STA.SMC controllers. The PI parameters used for the simulation were  $K_p = 8$  and  $K_i = 32$  established by the general characteristic closed-loop equations. The parameters for the two controllers, DPSTA.SMC and STA.SMC, were optimized using the trial-and-error method and set to  $K_1 = 35$ ,  $K_2 = 15$  and  $\lambda = 3/2$ . To ensure a fair comparison between the two sliding mode controllers, the gain values of  $K_1$  and  $K_2$  were kept the same for both controllers. Furthermore, in the future, genetic algorithm (GA) methods could be adopted to obtain optimal gain values for the DPSTA.SMC methods. We analyzed system’s behavior under the european driving cycle (EUDC). It consists of a simple extra-urban run of about 400 seconds which simulates driving at constant speed on an open road with a maximum speed of 120 km/h.

The Figure 4 illustrates the speed response of the four controllers: DPSTA.SMC, PI, STA, SMC, and FLSC. The speed error of the four strategies is shown in Figure 5. It is demonstrated that all controllers are capable of tracking the reference speed throughout the entire speed change range. The PI controller followed

the reference speed with a maximum error of 2.33 km/h. On the other hand, the FLSC showed a smaller error for the transient period when compared to the PI, but the steady-state error was 0.1 km/h. However, both SMC controllers exhibited better performances than the FLSC and PI controllers, achieving a speed error no greater than 0.01 km/h while tracking the desired reference speed.

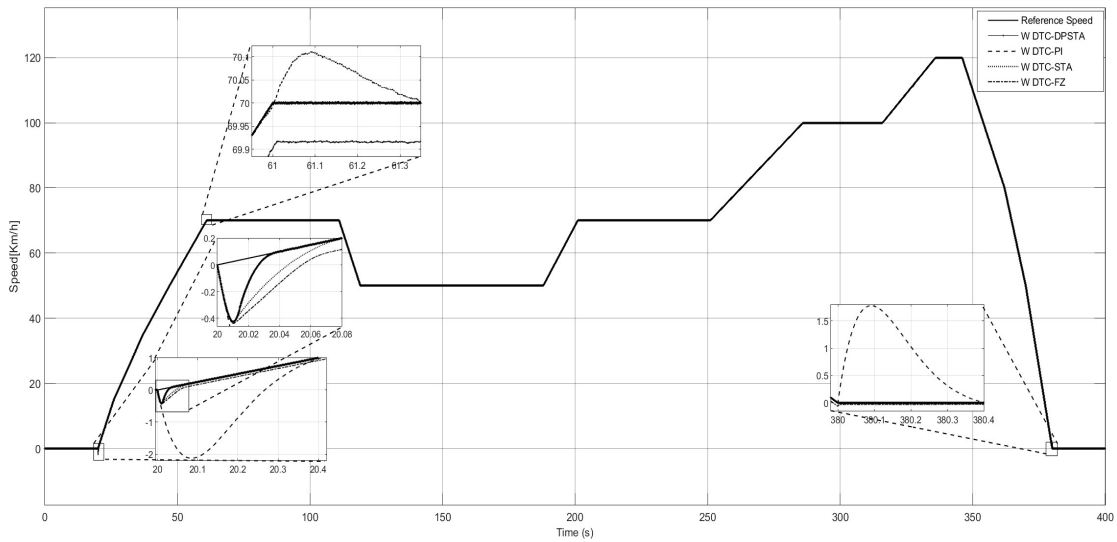


Figure 4. Evolution of the VE speed (Km/h) during the EUDC cycle

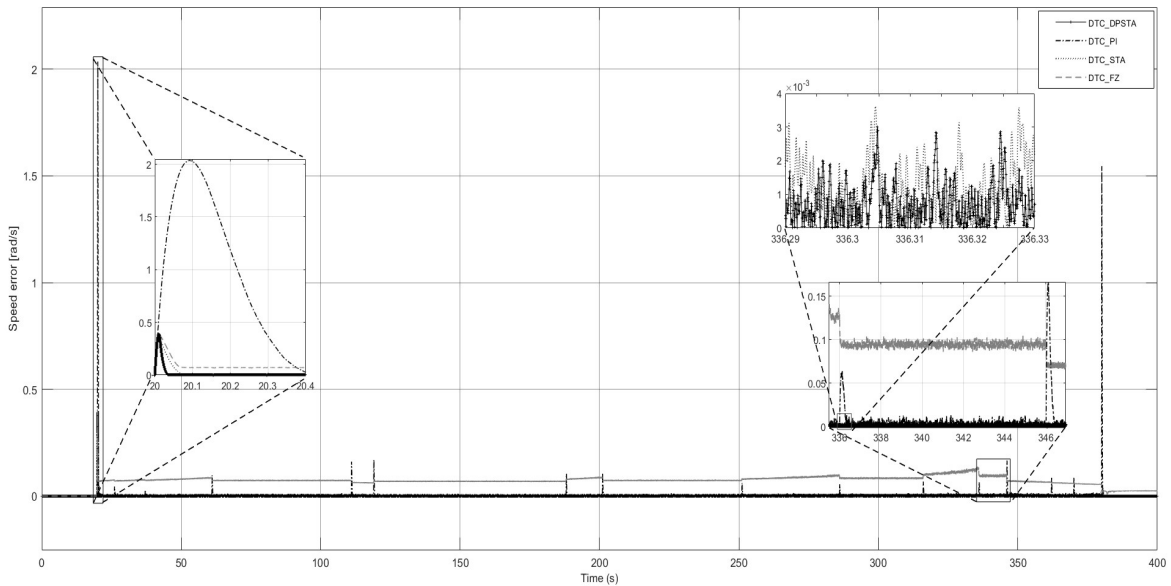


Figure 5. Evolution of the error speed (rad/s) during the EUDC cycle

Compared to the STA.SMC, the DPSTA.SMC controller provides significant improvements in the response speed and disturbance rejection performance of the vehicle speed control system. The proposed algorithm reduces the system response time by 57% during the startup state. In case of speed variations or load disturbances, DPSTA.SMC reduced the adjustment time to less than 60% compared with STA.SMC.



The chattering phenomenon produced by the SMC controller is manifested in the speed ripples. A comparison of the speed ripples amplitude of the two SMC controllers is shown in Table 3. A detailed analysis of the zoomed areas in Figure 5 and Table 3 shows that the DPSTA\_SMC controller significantly reduces chattering effects. The DPSTA controller reduces ripples to less than  $7,764.10^{-4}$  km/h in steady state when operating at a reference speed of 70 km/h, and to  $3,608.10^{-3}$  km/h when operating at a reference speed of 120 km/h. The control strategy proposed in this article has succeeded to significantly improve control performance in terms of response speed and system robustness, while reducing the chattering phenomenon.

Table 4 presents a comparison of the final SoC values for the four controllers in EUDC cycle. The DPSTA\_SMC controller maintained the SoC at 78,670%, while the FLSC and PI controllers were able to maintain it at a value less than 78,60%. These results clearly demonstrate the superiority of the DPSTA\_SMC controller over the other controllers. The speed controller proposed in this paper significantly improves the performance of the DTC control in terms of robustness to perturbations and energy efficiency.

Table 2. Simulation parameters

Parameters	Abbr.	Unit	Value	Parameters	Abbr.	Unit	Value
Induction Machine Parameters				Vehicle Parameters			
Rotor Inductance	$L_r$	$H$	0.0156	Vehicle mass	$m$	$Kg$	870
Stator Inductance	$L_s$	$H$	0.0156	Rolling Resistance Coefficient	$C_{rr}$		1
Mutual Inductance	$L_m$	$H$	0.2848	Gravitational Acceleration Constant	$g$	$m/s^2$	9.81
Stator Resistance	$R_s$	$Ohm$	4.1250	Air Density	$r$	$kg/m^3$	1.17
Rotor Resistance	$R_r$	$Ohm$	2.486	Frontal Area	$A_f$	$m^2$	2.64
Number of Pole Pairs	$p$	1	2	Aerodynamic Drag Constant	$C_d$		1
Motor Load Inertia	$J$	$Kg.m^2$	0.139	Transmission Ratio	$n$		1
Viscous Friction Coefficient	$f_v$	$N.m.s$	0.0095	Wheel radius	$R$	$m$	0.32
Battery Parameters							
Battery Configuration	$N_{Cell\_serie}$	1	96	Initial SoC	$SoC_0$	%	80
	$N_{Cell\_parallel}$	1	4	Nominal Battery Pack Energy	$E$	$KWh$	22

Table 3. Speed ripples amplitude for DPSTA\_SMC and STA\_SMC controllers

$v_{ref}(km/h)$	70	50	100	120
DPSTA_SMC	$7,764.10^{-4}$	$4,827.10^{-4}$	$7,768.10^{-3}$	$3,608.10^{-3}$
STA_SMC	$8,119.10^{-3}$	$7,059.10^{-3}$	$1,366.10^{-2}$	$2,048.10^{-2}$

Table 4. The end values of the SoC (%)

	DPSTA_SMC	PI	STA_SMC	FLSC
SoC (%)	78,670	78,659	78,669	78,653

## 5. CONCLUSION

In this article, a DPSTA\_SMC speed controller is designed based on the idea of replacing the switching function in the super-twisting algorithm with DPSMRL to overcome the limitations of the STA\_SMC controller in the context of DTC control of an MI used to EV driving. The structure of the EV, including MI and battery, was modeled and simulated to evaluate the controller performance using MATLAB tools. The performances of the proposed SMC are compared with that of PI, fuzzy logic, and traditional STA\_SMC controllers. The proposed DPSTA\_SMC speed controller offers significant advantages in terms of performance, state of charge stability and reduced chattering. These results pave the way for future improvements in electric vehicle control, aimed at maximizing efficiency, reliability, and durability.

## REFERENCES





- [1] S. F. Tie and C. W. Tan, "A review of energy sources and energy management system in electric vehicles," *Renewable and Sustainable Energy Reviews*, vol. 20, pp. 82–102, Apr. 2013, doi: 10.1016/j.rser.2012.11.077.

- [2] C. S. T. Dong, H. H. Le, and H. H. Vo, "Field oriented controlled permanent magnet synchronous motor drive for an electric vehicle," *International Journal of Power Electronics and Drive Systems*, vol. 14, no. 3, pp. 1374–1381, 2023, doi: 10.11591/ijpeds.v14.i3.pp1374-1381.
- [3] Q. Chen, C. Liao, A. Ouyang, X. Li, and Q. Xiao, "Research and development of in-wheel motor driving technology for electric vehicles," *International Journal of Electric and Hybrid Vehicles*, vol. 8, no. 3, pp. 242–254, 2016, doi: 10.1504/IJEHV.2016.080024.
- [4] A. Emadi, Y. J. Lee, and K. Rajashekara, "Power electronics and motor drives in electric, hybrid electric, and plug-in hybrid electric vehicles," *IEEE Transactions on Industrial Electronics*, vol. 55, no. 6, pp. 2237–2245, 2008, doi: 10.1109/TIE.2008.922768.
- [5] H. Bachiri, B. Gasbaoui, A. Ghezouani, and N. Nair, "Improved direct torque control strategy performances of electric vehicles induction motor," *International Journal of Power Electronics and Drive Systems*, vol. 13, no. 2, pp. 716–723, 2022, doi: 10.11591/ijpeds.v13.i2.pp716-723.
- [6] M. Zeraoulia, M. E. H. Benbouzid, and D. Diallo, "Electric motor drive selection issues for HEV propulsion systems: A comparative study," *IEEE Transactions on Vehicular Technology*, vol. 55, no. 6, pp. 1756–1764, 2006, doi: 10.1109/TVT.2006.878719.
- [7] S. Mencou, M. Ben Yakhlef, and E. B. Tazi, "Advanced Torque and Speed Control Techniques for Induction Motor Drives: A Review," in *2022 2nd International Conference on Innovative Research in Applied Science, Engineering and Technology, IRASET 2022*, 2022, pp. 1–9, doi: 10.1109/IRASET52964.2022.9738368.
- [8] M. Aktas, K. Awaili, M. Ehsani, and A. Arisoy, "Direct torque control versus indirect field-oriented control of induction motors for electric vehicle applications," *Engineering Science and Technology, an International Journal*, vol. 23, no. 5, pp. 1134–1143, 2020, doi: 10.1016/j.jestch.2020.04.002.
- [9] T. Sutikno, N. R. N. Idris, and A. Jidin, "A review of direct torque control of induction motors for sustainable reliability and energy efficient drives," *Renewable and Sustainable Energy Reviews*, vol. 32, pp. 548–558, 2014, doi: 10.1016/j.rser.2014.01.040.
- [10] S. K. Chien et al., "Enhanced DTC induction motor drives for THD minimization performance improvement with multilevel inverter," *International Journal of Power Electronics and Drive Systems*, vol. 13, no. 1, pp. 93–101, 2022, doi: 10.11591/ijpeds.v13.i1.pp93-101.
- [11] A. Shukla and R. Sharma, "Modified DTC with Adaptive Compensator for Low-Speed Region of Induction Motor in Electric Vehicle Applications," *Smart Science*, vol. 8, no. 3, pp. 101–116, 2020, doi: 10.1080/23080477.2020.1795342.
- [12] I. Takahashi and T. Noguchi, "A New Quick-Response and High-Efficiency Control Strategy of an Induction Motor," *IEEE Transactions on Industry Applications*, vol. IA-22, no. 5, pp. 820–827, 1986, doi: 10.1109/TIA.1986.4504799.
- [13] M. H. N. Talib et al., "An improved simplified rules Fuzzy Logic Speed Controller method applied for induction motor drive," *ISA Transactions*, vol. 105, pp. 230–239, 2020, doi: 10.1016/j.isatra.2020.05.040.
- [14] P. Alkorta, J. A. Cortajarena, O. Barambones, and F. J. Maseda, "Effective generalized predictive control of induction motor," *ISA Transactions*, vol. 103, pp. 295–305, 2020, doi: 10.1016/j.isatra.2020.04.008.
- [15] F. Kadri and M. A. Hamida, "Neural Direct Torque Control for Induction Motor under Voltage Source Inverter Open Switch Fault," *Recent Advances in Electrical and Electronic Engineering (Formerly Recent Patents on Electrical and Electronic Engineering)*, vol. 13, no. 4, pp. 571–579, 2019, doi: 10.2174/1874476105666190830103616.
- [16] S. Mencou, M. Ben Yakhlef, and E. B. Tazi, "Fuzzy Logic Speed Controller for Robust Direct Torque Control of Induction Motor Drives," *Lecture Notes in Networks and Systems*, vol. 668 LNNS, pp. 601–611, 2023, doi: 10.1007/978-3-031-29857-860.
- [17] F. Shiravani, P. Alkorta, J. A. Cortajarena, and O. Barambones, "An Enhanced Sliding Mode Speed Control for Induction Motor Drives," in *Actuators*, 2022, vol. 11, no. 1, p. 18, doi: 10.3390/act11010018.
- [18] N. V. Quan and M. T. Long, "Sensorless sliding mode control method for a three-phase induction motor," *Electrical Engineering*, vol. 104, no. 5, pp. 3685–3695, 2022, doi: 10.1007/s00202-022-01578-5.
- [19] Y. Feng, X. Yu, and F. Han, "On nonsingular terminal sliding-mode control of nonlinear systems," *Automatica*, vol. 49, no. 6, pp. 1715–1722, 2013, doi: 10.1016/j.automatica.2013.01.051.
- [20] S. E. Farhi, D. Sakri, and N. Golea, "High-performance induction motor drive based on adaptive super-twisting sliding mode control approach," *Archives of Electrical Engineering*, vol. 71, no. 1, pp. 245–263, 2022, doi: 10.24425/ae.2022.140208.
- [21] Y. Feng, F. Han, and X. Yu, "Chattering free full-order sliding-mode control," *Automatica*, vol. 50, no. 4, pp. 1310–1314, 2014, doi: 10.1016/j.automatica.2014.01.004.
- [22] K. D. Young, V. I. Utkin, and U. Ozguner, "A control engineers guide to sliding mode control," *IEEE Transactions on Control Systems Technology*, vol. 7, no. 3, pp. 328–342, 1999, doi: 10.1109/87.761053.
- [23] W. Perruquetti and J.P. Barbot, *Sliding Mode Control In Engineering*. CRC press, 2002.
- [24] S. Vaidyanathan and C. H. Lien, *Applications of sliding mode control in science and engineering*, vol. 709. Springer, 2017.
- [25] Y. Shtessel, C. Edwards, L. Fridman, and A. Levant, *Sliding Mode Control and Observation*, vol. 10. New York, NY: Springer New York, 2014.
- [26] L. Fridman, J. A. Moreno, B. Bandyopadhyay, S. Kamal, and A. Chalanga, "Continuous nested algorithms: The fifth generation of sliding mode controllers," *Studies in Systems, Decision and Control*, vol. 24, pp. 5–35, 2015, doi: 10.1007/978-3-31918290-22.
- [27] Y. Yang, Y. Yan, and X. Xu, "Fractional order adaptive fast super twisting sliding mode control for steer by wire vehicles with time delay estimation," *Electronics (Switzerland)*, vol. 10, no. 19, p. 2424, 2021, doi: 10.3390/electronics10192424.
- [28] I. Sami, S. Ullah, A. Basit, N. Ullah, and J. S. Ro, "Integral super twisting sliding mode based sensorless predictive torque control of induction motor," *IEEE Access*, vol. 8, pp. 186740–186755, 2020, doi: 10.1109/ACCESS.2020.3028845.
- [29] A. Levant, "Sliding order and sliding accuracy in sliding mode control," *International Journal of Control*, vol. 58, no. 6, pp. 1247–1263, 1993, doi: 10.1080/00207179308923053.
- [30] A. Levant, "Principles of 2-sliding mode design," *Automatica*, vol. 43, no. 4, pp. 576–586, 2007, doi: 10.1016/j.automatica.2006.10.008.
- [31] J. A. Moreno and M. Osorio, "A Lyapunov approach to second-order sliding mode controllers and observers," in *Proceedings of the IEEE Conference on Decision and Control*, 2008, pp. 2856–2861, doi: 10.1109/CDC.2008.4739356.
- [32] M. Tao, Q. Chen, X. He, and M. Sun, "Adaptive fixed-time fault-tolerant control for rigid spacecraft using a double power reaching law," *International Journal of Robust and Nonlinear Control*, vol. 29, no. 12, pp. 4022–4040, 2019, doi: 10.1002/rnc.4593.
- [33] H. J. Li and Y. L. Cai, "Sliding mode control with double power reaching law," *Kongzhi yu Juece/Control and Decision*, vol. 31, no. 3, pp. 498–502, 2016, doi: 10.13195/j.kzyjc.2014.1908.





- [34] M. Ehsani, *Modern Electric, Hybrid Electric, and Fuel Cell Vehicles*, Third Edition. CRC Press, 2018.
- [35] W. Zhou, Y. Zheng, Z. Pan, and Q. Lu, "Review on the battery model and SOC estimation method," *Processes*, vol. 9, no. 9, p. 1685, 2021, doi: 10.3390/pr9091685.
- [36] K. S. Ng, C.-S. Moo, Y.-P. Chen, and Y.-C. Hsieh, "Enhanced coulomb counting method for estimating state-of-charge and state-of-health of lithium-ion batteries," *Applied Energy*, vol. 86, no. 9, pp. 1506–1511, Sep. 2009, doi: 10.1016/j.apenergy.2008.11.021.
- [37] R. Marino, P. Tomei, and C. M. Verrelli, "Induction Motor Control Design," *Journal of Chemical Information and Modeling*, vol. 53, no. 9, pp. 1689–1699, 2010, [Online]. Available: <http://link.springer.com/10.1007/978-1-84996-284-1>.

## BIOGRAPHIES OF AUTHORS







**Siham Mencou**     was born in 1996 in Boulemane, Morocco. She obtained her engineering master's degree in electromechanics in 2019 from the National School of Mines in Rabat, Morocco. Currently, she is actively pursuing her Ph.D. at the Laboratory of Engineering Sciences, Polydisciplinary Faculty of Taza, Sidi Mohamed Ben Abdellah University, Fez, Morocco. Her research focuses on artificial intelligence, control systems, and electric vehicle drive systems. She can be contacted at email: [siham.mencou@usmba.ac.ma](mailto:siham.mencou@usmba.ac.ma).



**Majid Ben Yakhlef**     defended his doctoral thesis in computer science and automation at the University Sidi Mohamed Ben Abdellah (USMBA) Morocco. He was recruited in 2007 as a lecturer at the Faculty of Taza; he defended his HDR in 2012 following the research work he carried out at the LIMA O laboratory. Ben Yakhlef does his research in computer engineering, control systems engineering and artificial intelligence. Currently a member of the Engineering Sciences Laboratory. In recent years, his work has shifted towards data sciences. He can be contacted at email: [majid.benyakhlef@usmba.ac.ma](mailto:majid.benyakhlef@usmba.ac.ma).



**Elbachir Tazi**     graduated in electronic engineering from ENSET Mohammedia Morocco in 1992. He obtained his DEA and DES in automation and signal processing and his Ph.D. in computer science from Sidi Mohammed Ben Abdellah University (USMBA), faculty of sciences in Fez, Morocco respectively in 1995, 1999 and 2012. He is now a member of the engineering sciences laboratory and associate professor at USMBA University, Polydisciplinary Faculty of Taza, Morocco. His research focuses on Automatic Speaker Recognition Systems Applications and as well as automatic control systems based on artificial intelligence methods. He can be contacted at email: [elbachir.tazi@usmba.ac.ma](mailto:elbachir.tazi@usmba.ac.ma).